Pakistan Veterinary Journal

ISSN: 0253-8318 (PRINT), 2074-7764 (ONLINE)
DOI: 10.29261/pakvetj/2026.182

RESEARCH ARTICLE

Total Flavonoids of *Lophatherum gracile* Alleviate Pseudorabies Virus Induced Inflammation by Modulating NF-κB/MAPK Signaling and TCA Cycle-Related Metabolism

Cheng Zeng[1†], Xiaodie Li[1†], Liting Cao[2], Anchun Cheng[1], Zhentao Cheng[1], Ying Chen[1], Qing Liu[3], Luqing Yang[1], Jian Yang[1*] and Xuqin Song[1*]

[1]Institute of Veterinary Medicine and Immunology Drugs, Veterinary Department in College of Animal Science, State Key Laboratory of Green Pesticide, GuiZhou University, Guiyang 550025, China; [2]Department of Traditional Chinese Veterinary Medicine, College of Veterinary Medicine, Southwest University, Rongchang, Chongqing, 402460, China; [3]The Yunnan Key Laboratory of Veterinary Etiological Biology, College of Veterinary Medicine, Yunnan Agricultural University, Kunming, 650201, China. †The authors contributed equally to this work
*Corresponding author: yangjian0104@163.com (JY); song1991yi@163.com (XS)

ARTICLE HISTORY (26-773)

Received: June 26, 2026
Revised: August 16, 2026
Accepted: August 18, 2026
Published online: August 28, 2026

Key words:
Anti-inflammatory effect
Flavonoids of *Lophatherum gracile*
Metabolomics
NF-κB/MAPK signaling pathway
Porcine pseudorabies virus

ABSTRACT

Pseudorabies virus (PRV) infection induces severe inflammatory injury and tissue damage. Total flavonoids of *Lophatherum gracile* (TFLG) exert excellent anti-inflammation effects, it alleviates the inflammatory damage caused by PRV infection remains unclear. Here, RAW264.7 cells and mouse models were used to evaluate the protective effects of TFLG on PRV-induced inflammatory injury and to clarify its underlying mechanism. Results showed that TFLG had no cytotoxicity at 0.025–0.1mg/mL and significantly improved the viability of PRV-infected cells. In PRV-infected mice, TFLG reduced abnormal increases in inflammatory cells and improved organ indices and histopathological injury. In RAW264.7 cells and mice, TFLG markedly reduced NO release and inhibited the production and mRNA levels of *IL-1β*, *IL-6* and *TNF-α*. Meanwhile, TFLG increased *IL-10* expression. Moreover, TFLG restrained PRV-mediated NF-κB/MAPK pathways activation, accompanied by reduced phosphorylation of p65, IκBα, p38 and JNK. Untargeted metabolomics further revealed that PRV caused marked metabolic disorders in cells and mouse serum, whereas TFLG partially recovered these metabolic changes. TCA cycle was a common metabolic pathway involved in the protective effect of TFLG. The correlation analyses suggested that TFLG may attenuate inflammation by regulating glutamine/glutamate-derived α-ketoglutarate metabolism, thereby relieving the inflammatory activation mediated by NF-κB/MAPK signaling pathway. This study provides new evidence that TFLG alleviates PRV-induced inflammatory injury through regulating metabolic–immune axis, which will contribute to TFLG as a promising natural candidate for the prevention and control of virus-associated inflammatory damage.

To Cite This Article: Zeng C, Li X, Cao L, Cheng A, Cheng Z, Chen Y, Liu Q, Yang L, Yang J and Song X, 2026. Total flavonoids of *Lophatherum gracile* alleviate Pseudorabies virus induced inflammation by modulating NF-κB/MAPK signaling and TCA cycle-related metabolism. Pak Vet J, 46(8): 2136-2146. http://dx.doi.org/10.29261/pakvetj/2026.182

INTRODUCTION

As the etiological agent of Aujeszky's disease, pseudorabies virus (PRV) belongs to the Alphaherpesvirinae subfamily and contains a double-stranded DNA genome. Pigs are primary natural hosts, but the virus can infect diverse mammals and may cause lethal disease in non-porcine species (Zhuang *et al.,* 2025). In swine, PRV leads to reproductive failure in sows, neurological disease in piglets and respiratory disorders in growing pigs. Although vaccination has reduced the occurrence of diseases, PRV remains difficult to eliminate because of the emergence of wild-type, variant and recombinant strains (Yao *et al.,* 2022). Recent evidence indicates that PRV has caused substantial economic losses in the global breeding industry (Bo and Li, 2022; Liu *et al.,* 2022a). A meta-analysis reported an overall PRV seroprevalence of 21.5% in China, indicating its continuous transmission despite vaccination (Gao *et al.,* 2025). Vaccination alone may not provide sufficient protection under current production conditions, so complementary antiviral strategies should be to reduce viral injury.

PRV pathogenesis is not limited to viral replication. Many studies suggest that PRV can induce excessive inflammation, immune dysregulation, and metabolic disorders in infected tissues and cells (Chen *et al.,* 2025). NF-κB and MAPK signaling are central mediators of the inflammatory response during PRV infection. The NF-κB pathways are primarily regulated by p65/RelA and p50. Once translocated into the nucleus, p65 drives the expression of genes encoding pro-inflammatory cytokines. For instance, PRV activates the TLR/NF-κB signaling pathways and the AIM2 inflammasome, promoting the production of IL-1β, IL-6 and TNF-α (Zhou *et al.,* 2023). MAPK signaling, especially p38 MAPK, also contributes to the production of pro-inflammatory cytokines and can interact with the NF-κB pathways (Yang *et al.,* 2026). Meanwhile, pro-inflammatory cytokines further activate p38 MAPK, amplifying the inflammatory response (Vervaeke and Lamkanfi, 2025). In addition, recent studies indicate that PRV infection significantly disrupts host metabolic homeostasis. PRV can change many metabolic processes such as glycolysis, glutamine, lipid, and nucleotide metabolism, which is beneficial to viral synthesis and replication (Liu *et al.,* 2022b). More importantly, integrated transcriptomic and metabolomic analyses reveal that differential metabolites in PRV-infected mice are closely associated with inflammation-related pathways (e.g., TNF and PI3K-Akt) (Xu *et al.,* 2024). Thus, agents that simultaneously restrain inflammatory injury and recover metabolic balance may provide broader protection than antiviral strategies targeting viral replication alone.

Natural products have attracted increasing attention as complementary agents against virus-induced inflammatory injury. Natural bioactive compounds can control PRV-associated damage. Ginkgolic acid, for instance, reduces PRV replication both *in vitro* and *in vivo* by interfering with viral late gene transcription (Bo *et al.,* 2023). *Arthrospira platensis* polysaccharide alleviated PRV-induced inflammation in RAW264.7 cells and mouse lung tissues. *Glycyrrhiza* polysaccharides also reduced PRV-related injury in mice through adjusting inflammation, oxidative status, intestinal barrier function, and gut microbial balance (Song *et al.,* 2025). *Lophatherum gracile* is a medicinal and food homologous herb that has long been used as herbal tea to promote diuresis and relieve inflammatory symptoms (Chen *et al.,* 2023a; Li *et al.,* 2024). Phytochemical studies have confirmed that *Lophatherum gracile* is rich in flavonoids, with vitexin, isovitexin, and luteolin as major active constituents (Tang *et al.,* 2015). Pharmacological research has shown that the total flavonoids of *Lophatherum gracile* (TFLG) have antioxidant, anti-inflammatory, and antiviral activities (Chen *et al.,* 2023b). Our earlier findings confirmed that TFLG reduced LPS-induced inflammation through multi-target mechanisms involving inflammatory signaling (Li *et al.,* 2025). These results demonstrate that the TFLG could modulate PRV-induced inflammatory injury and metabolic disorders, while its protective effect and mechanism of action during PRV infection remain unclear.

To clarify the mechanisms by which TFLG alleviates PRV-induced injury, we established *in vitro* and *in vivo* inflammatory models using PRV-infected RAW264.7 cells and mice. We further evaluated the regulatory role of TFLG in NF-κB/MAPK mediated inflammatory responses. Next, untargeted metabolomics was applied to analyze TFLG-regulated metabolic pathways in infected cells and mice. Finally, correlations among inflammatory cytokines, NF-κB/MAPK-related proteins, and differential metabolites were analyzed to clarify the association between inflammation and metabolic remodeling after TFLG treatment.

MATERIALS AND METHODS

Materials and reagents: DMEM (BM0003) and fetal bovine serum (FBS; Z7010FBS-500) were purchased from ZETAlife (CA, USA). Dexamethasone (DEX) was obtained from Yuanye Biotechnology Co., Ltd. (Shanghai, China). ELISA kits for inflammatory factors were supplied by Yuanju Biotechnology Center Co., Ltd. (Shanghai, China). Total RNA extraction kits and cDNA reverse-transcription were obtained from Novozymes Biotechnology Co., Ltd. (Nanjing, China). CCK-8 kits were provided by Meilun Biotechnology Co., Ltd. (Dalian, China). Antibodies were supplied by Cell Signaling Technology (MA, USA). Glycine, Tris, sodium dodecyl sulfate (SDS), penicillin-streptomycin solution, and 0.25% trypsin were purchased from Solarbio (Beijing, China). PRV and RAW264.7 cells were donated by the Veterinary Pharmacology Laboratory, College of Animal Science and Technology, Guangxi University. TFLG was extracted and characterized as described in the study (Li *et al,.* 2025).

Cell culture and viability assay: PK-15 and RAW264.7 cells were cultured in DMEM with 10% FBS at 37°C in a 5% CO_2 incubator. PRV was amplified in PK-15 cells and stored at −80°C. Viral titres were estimated according to the Reed-Muench method, and the $TCID_{50}$ was calculated as $10^{-5.9}$/0.1mL (Table S1). For cell experiments, RAW264.7 cells were divided into control groups (CK), PRV-infection group, TFLG treatment group (PRV-infected cells treated with 0.025, 0.05 and 0.1mg/mL TFLG) and DEX treatment group (PRV-infected cells treated with 0.5mg/mL dexamethasone). Once the cell monolayer reached nearly 80% confluence, CCK-8 was performed according to the guidelines of manufacturer. The absorbance at 450nM was used to calculate relative cell viability against the control group.

Animal experiment design: SPF Kunming mice [SCXK (Yu) 2020-0005] were supplied by Henan Skobase Biotechnology (Anyang, China). All animal procedures were conducted under the approval of the Animal Experimental Committee of Guizhou University (EAE-GZU-2023-E073) and complied with institutional guidelines for animal care and welfare. Mice can be accessed to food and water during the experiment. After 7 days of acclimation, the animals were randomly allocated into six groups, including the control (CK) group, PRV-infection group (10^{-4} dilution of PRV, 100μL/mouse), TFLG treatment groups (100, 300 and 500mg/kg) and DEX treatment group (5mg/kg of dexamethasone), with six mice per group. Except for the control group, which

was administered DMEM, mice were intramuscularly inoculated with PRV. Six hours after infection, mice were treated with the corresponding drugs via oral gavage once daily for 7 days, whereas the CK and PRV groups received same volume of normal saline. Six hours after the final administration, body weight was recorded, and mice were anaesthetized with isoflurane. Blood, liver, spleen, lung, kidney and brain samples were collected for subsequent analyses.

Histopathological analysis: Lung, brain and spleen tissues were rinsed with normal saline, preserved in 4% paraformaldehyde, dehydrated, paraffin embedded, and sectioned. After haematoxylin and eosin (HE) staining and dehydration, tissue sections were observed under a light microscope.

Determination of inflammatory cytokines and NO levels: Inflammatory cytokine and NO levels were measured in cell culture supernatants and mouse serum. For inflammatory cytokines and NO levels, samples were evaluated based on the kit instructions. After adding 100μL of HRP-conjugated antibody to the standard and sample wells, the plate was kept at 37°C for 60 min. Then, 50μL of substrate solution was added to each well and reacted for 15min. After addition of 50μL stop solution, IL-1β, IL-6, IL-10 and TNF-α levels were detected at 450nM.

The expression levels of inflammatory cytokine genes: The qRT-PCR was used to quantify *IL-6*, *IL-10*, *IL-1β*, and *TNF-α* mRNA levels in cells and mouse lung tissues. Lung tissues and cell samples were incubated with lysis buffer on ice for 30 min. Total RNA was extracted using the Total RNA Kit, followed by cDNA synthesis with a reverse-transcription kit. The PCR reaction system consisted of 10.0μL SYBR qPCR Master Mix, 0.4μL upstream primer, 0.4μL downstream primer, 1.8μL Template DNA/cDNA and 7.4μL ddH_2O. The PCR cycling conditions were as follows: 95°C for 30s, 95°C for 5s, 56°C for 10s, 72°C for 18s, a total of 40 cycles and extension at 65°C for 20s. Relative expression of inflammation-related genes was determined using $2^{-\triangle\triangle Ct}$ method. Primer sequences are provided in Tables S2 and S3.

Analysis of NF-κB and MAPK signaling pathways proteins by western blotting: 20mg of lung tissue was ground at low temperature. Lung and cell samples were lysed on ice with lysis buffer for 30min. Protein concentration was measured with the BCA Kit following the instructions of manufacturer and samples were normalized to equal protein concentrations. Proteins were resolved on 12% SDS-PAGE at 80 V for 30min, followed by 120V for 1h. Proteins were then transferred onto PVDF membranes with a semi-dry blotting system at 25V for 5min. Membranes were treated with 5% skimmed milk for 2h to block nonspecific binding and exposed to primary antibodies overnight at 4°C. The membranes were rinsed three times with TBST before treatment with secondary antibody for 2h. Protein bands were detected with an ECL chemiluminescence kit, scanned and analyzed using ImageJ software. The relative expression level of each target protein was determined by densitometric analysis of the protein bands using ImageJ software and normalized to β-actin. The normalized protein expression level in the control group was set to 1.

Metabolomics analysis: Cell and serum samples were extracted by pre-cooled methanol/acetonitrile (1:1, v/v) spiked with isotope-labelled internal standards and incubated at −20°C for 10min. Samples were centrifuged and supernatants were dried under vacuum and reconstituted before analysis. Target compounds were separated and identified by ultra-performance liquid chromatography-high resolution mass spectrometry (UPLC-HRMS). Separation was achieved on an ACQUITY UPLC BEH Amide column (1.7μM, 2.1mM×100mM; Waters Corporation, USA) under gradient elution using acetonitrile and a 25 mmol/L ammonium acetate–25 mmol/L ammonium hydroxide buffer at pH 9.0. Analysis was carried out using a Vanquish UHPLC system coupled with an Orbitrap Exploris 120 HRMS (Thermo Fisher Scientific, USA), with an injection volume of 2μL. MS data were obtained using Xcalibur 4.4 software in positive/negative ion mode, with simultaneous collection of MS and MS/MS data. ProteoWizard was used to convert raw files into mzML format, after which metabolite annotation and visualization were completed in R.

Date analysis: Statistical analyses were conducted with GraphPad Prism version 9.5.0. Differences among groups were evaluated by one-way analysis of variance (ANOVA), followed by least significant difference (LSD) tests for pairwise comparisons. Results are expressed as the mean ± standard deviation (mean ± SD).

RESULTS

Screen of TFLG dose and its effect on the cell viability of RAW264.7: TFLG at 0.025, 0.05 and 0.1mg/mL significantly promoted cell growth ($P<0.05$), whereas 0.2mg/mL or higher TFLG markedly reduced cell viability ($P<0.01$) (Fig. 1A). Therefore, 0.025, 0.05 and 0.1mg/mL TFLG were selected for subsequent cell experiments. The effects of different PRV concentrations on cell viability are shown in Fig. 1B. Cell viability decreased progressively with increasing concentrations of PRV. In comparison with control group, PRV infection began to significantly reduce cell viability with its concentration higher than 10^{-3} ($P<0.05$). Notably, 10^{-2} PRV reduced cell viability by approximately 50% ($P<0.01$) and was therefore used to establish the PRV-induced inflammatory cell model. Treatment with TFLG significantly improved the viability of cells exposed to PRV (Fig. 1C). In comparison with PRV-treated group, the concentration of TFLG higher than 0.05mg/mL produced a highly significant increase in cell viability ($P<0.01$), with an effect comparable to that of dexamethasone. Therefore, TFLG showed no cytotoxicity to RAW264.7 cells at the selected concentrations and helped protect cells from PRV-related injury.

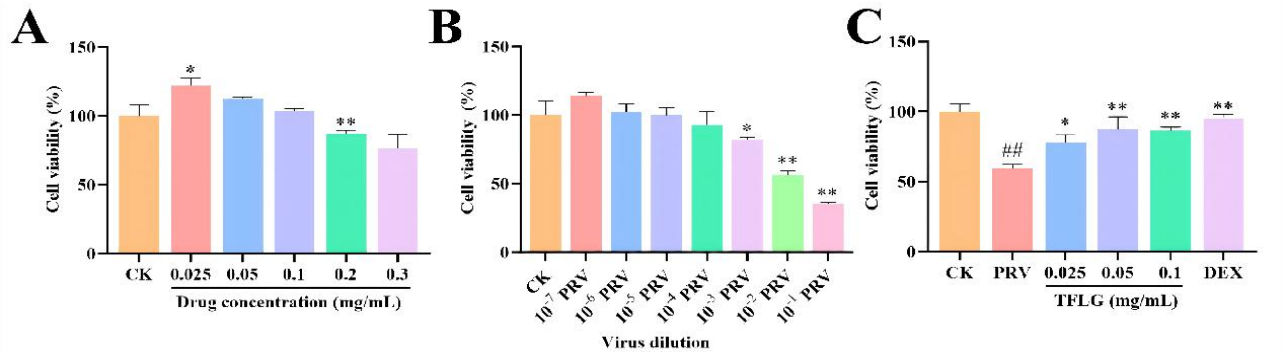

Fig. 1: Effects of (A) TFLG and (B) PRV on cell viability; (C) protective effect of TFLG on the viability of PRV-infected RAW264.7 cells. # represents comparison with the control group, and * represents comparison with the model group. ##P<0.01; *P<0.05; **P<0.01.

Effects of TFLG on inflammatory cells, organ indices and histopathology in PRV-infected Mice: Changes in inflammatory blood cell counts in PRV-infected mice after TFLG treatment are presented in Fig. 2A-D. PRV significantly elevated the proportions of white blood cells, neutrophils, lymphocytes and monocytes (P<0.01). However, TFLG treatment significantly reduced these inflammatory cell populations (P<0.05), indicating that TFLG attenuated the abnormal elevation of peripheral inflammatory cells induced by PRV. Although dexamethasone reduced some inflammatory cell populations, it markedly increased the proportion of neutrophils and strongly suppressed lymphocytes (P<0.01). Organ index analysis showed that PRV had significantly increased lung, spleen and brain indices, whereas the liver index tended to increase without statistical significance and the kidney index showed slight changes (Fig. 2E). After TFLG treatment, most abnormally elevated organ indices were reduced, indicating that TFLG alleviated PRV-induced organ swelling or pathological injury. In addition, 5mg/kg dexamethasone induced severe splenic atrophy in mice, which may be associated with its immunosuppressive effect.

Histopathological changes in mouse tissues were given in Fig. 2F. The control mice showed well-organized alveolar architecture, and no obvious lung injury was observed. After PRV infection, extensive inflammatory cell infiltration was observed in the alveolar wall, accompanied by alveolar wall thickening, widened alveolar septa, and collapse or disappearance of many alveoli. Both TFLG and dexamethasone could alleviate lung injury induced by PRV, with the high-dose TFLG showing the most pronounced protection. In the brain, the control group showed regularly arranged meningeal connective tissue, abundant and evenly distributed cortical neurons, and no obvious glial cell proliferation. PRV caused mild atrophy of hippocampal neurons and pyramidal cells, with blurred cell boundaries. TFLG treatment recovered the normal cellular morphology. In the spleen, the control group showed a normal capsule composed of dense connective tissue rich in elastic and smooth muscle fibres, with trabeculae extending into the splenic parenchyma. PRV infection reduced the amount of white pulp and caused diffuse distribution of blood cells and granulocyte infiltration. TFLG reduced granulocyte infiltration. Thus, TFLG reduced PRV-induced inflammatory cell abnormalities in peripheral blood and alleviated inflammatory infiltration and histopathological damage in the lung, spleen and brain.

Effects of TFLG on NO and inflammatory cytokines in *in-vitro* and *in-vivo*: Fig. 3A presents the changes in NO production, cytokine release, and cytokine gene expression in PRV-infected RAW264.7 cells. PRV significantly increased the production of NO and pro-inflammatory cytokines (IL-1β, IL-6 and TNF-α), while markedly suppressing IL-10 secretion (P<0.01). RT-qPCR analysis further showed that PRV infection significantly upregulated *IL-1β*, *IL-6* and *TNF-α* mRNA expression (P<0.01) and dramatically downregulated *IL-10* mRNA expression (P<0.05). After TFLG intervention, PRV-induced increases in NO, IL-1β, IL-6 and TNF-α were reduced, whereas IL-10 levels were significantly increased. The regulatory pattern of TFLG was observed like that in the dexamethasone group. TFLG also reversed the abnormal mRNA expression of inflammatory cytokines induced by PRV, with no significant difference from dexamethasone.

The effects of TFLG on serum NO and cytokine levels in mouse serum, as well as cytokine mRNA expression in mouse lungs, were shown in Fig. 3B. The *in-vivo* results were highly consistent with the findings from the RAW264.7 cells experiment. PRV infection significantly increased serum NO and pro-inflammatory cytokine levels, reducing IL-10 levels, upregulating pro-inflammatory cytokine mRNA expression and downregulating *IL-10* mRNA expression. TFLG treatment improved these abnormal changes. Accordingly, TFLG inhibited PRV-induced NO production both *in vitro* and *in vivo*, downregulated IL-1β, IL-6 and TNF-α levels, and upregulated IL-10, thereby reducing PRV-induced inflammatory responses.

Influence of TFLG on NF-κB and MAPK pathways proteins in *in-vitro* and *in-vivo* inflammatory models: To investigate the anti-inflammatory mechanism of TFLG *in-vitro* and *in-vivo*, Western blotting was used to reveal changes in proteins associated with the NF-κB and MAPK signaling pathways. In comparison with CK group, PRV challenge strongly increased the levels of phosphorylated p65 and IκBα in RAW264.7 cells (Fig. 4A), indicating the enhancement of the NF-κB pathways. Both TFLG and dexamethasone markedly reduced p65 and IκBα phosphorylation (P<0.01), with TFLG showing stronger inhibition than dexamethasone. Additionally, TFLG

significantly reduced PRV-induced phosphorylation of p38 and JNK ($P<0.01$), indicating the inhibition of the MAPK pathways induced by PRV (Fig. 4B). The *in-vivo* results showed a similar trend. PRV activated the NF-κB pathways in lung tissue, whereas TFLG reversed this effect (Fig. 4C). TFLG also significantly inhibited the phosphorylation of p38 and JNK in lung tissue induced by PRV ($P<0.01$), further suppressing the MAPK pathways (Fig. 4D). Thus, TFLG reduced the overactivation of the NF-κB and MAPK pathways induced by PRV both *in-vitro* and *in-vivo* by reducing the phosphorylation of p65, IκBα, p38 and JNK, thereby exerting anti-inflammatory and protective effects.

Principal component analysis: PCA was performed to evaluate the metabolic profiles of cell and serum samples. The QC samples formed tight clusters, and all samples were distributed within the 95% confidence region. In the cell model, the PRV group was clearly separated from the CK group, suggesting that PRV infection markedly altered intracellular metabolism. After TFLG treatment, the metabolic profile changed toward the CK group, consistent with a partial recovery of PRV-disrupted cellular metabolism (Fig. S1A). A similar trend was observed in mouse serum samples. The TFLG group was clearly separated from the PRV group, with a distribution pattern closer to that of the CK group, demonstrating that TFLG alleviated PRV-induced serum metabolic disturbances (Fig. S1B). The OPLS-DA models showed good fitting and predictive performance, with R^2Y values ranging from 0.995 to 0.999 and Q^2 values ranging from 0.547 to 0.683 where available (Fig. S1C–F). The 200-permutation tests supported the reliability of these models, confirming their suitability for subsequent screening of differential metabolites (Fig. S1G–J).

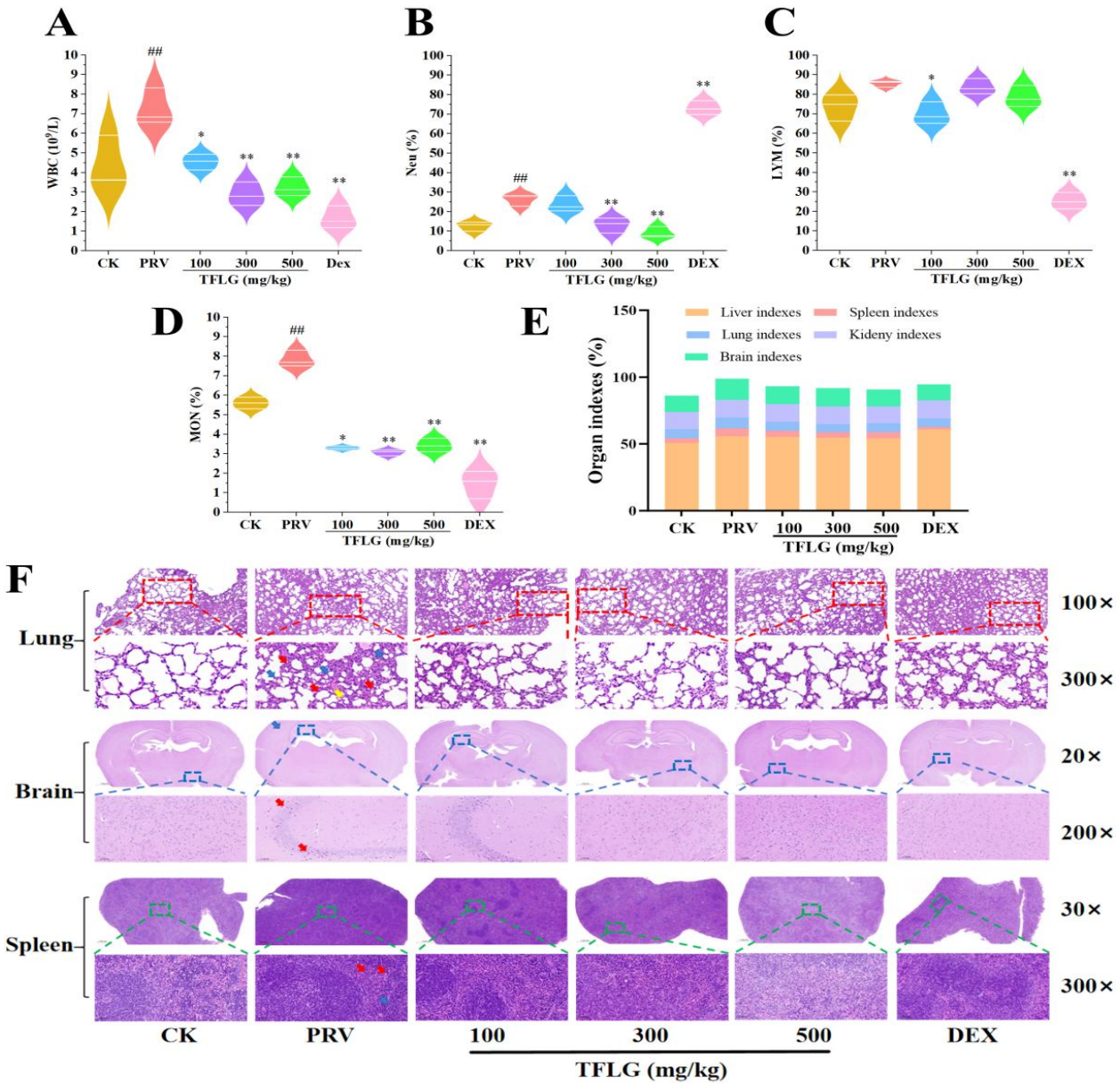

Fig. 2: Effects of TFLG on (A) white blood cells (WBCs), (B) neutrophils (Neu), (C) lymphocytes (Lym) and (D) monocytes (Mon) in the blood of PRV-infected mice, and on (E) organ indices and (F) histopathological changes in PRV-infected mice. In lung tissue, yellow arrows indicate monocytes, blue arrows indicate lymphocytes and red arrows indicate neutrophils. In brain tissue, blue arrows indicate neurons and red arrows indicate pyramidal cells. In spleen tissue, blue arrows indicate blood cells and red arrows indicate granulocytes. The indications of significant differences are shown in Fig. 1.

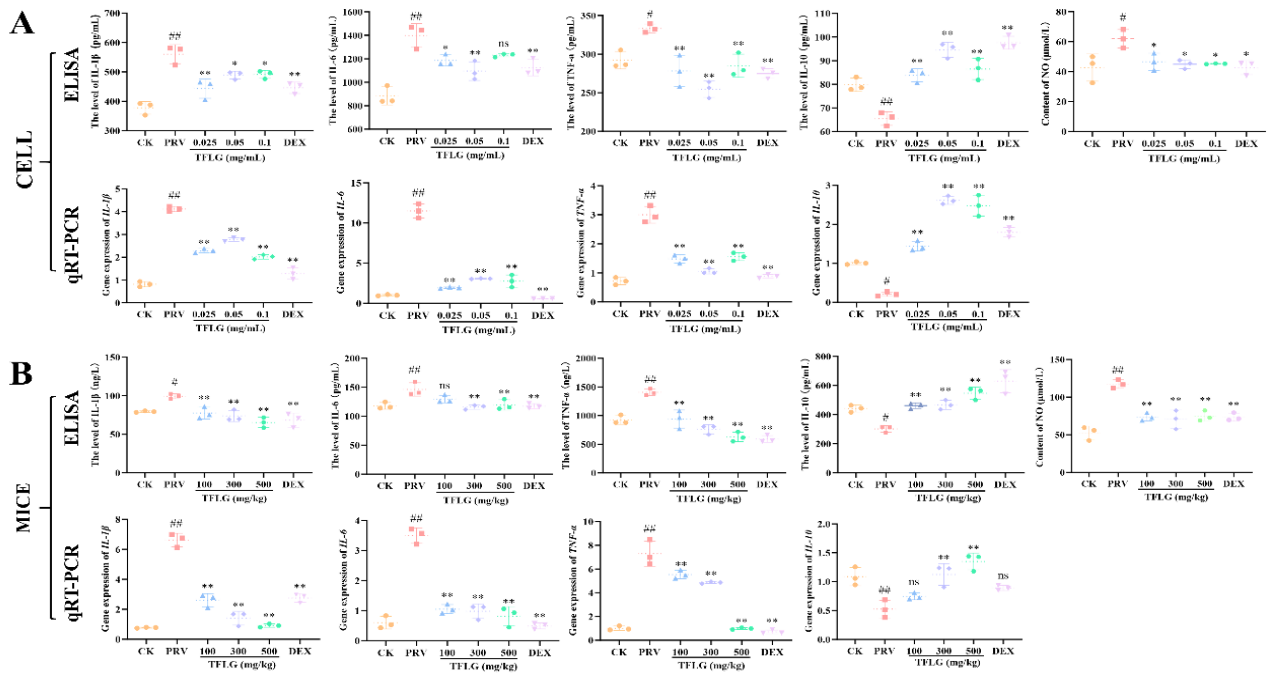

Fig. 3: Effects of TFLG on NO levels, inflammatory cytokine levels (IL-1β, IL-6, TNF-α and IL-10) and cytokine gene expression in (A) the PRV-induced cell infection model and (B) the PRV-induced mouse infection model. The indications of significant differences are shown in Fig. 1.

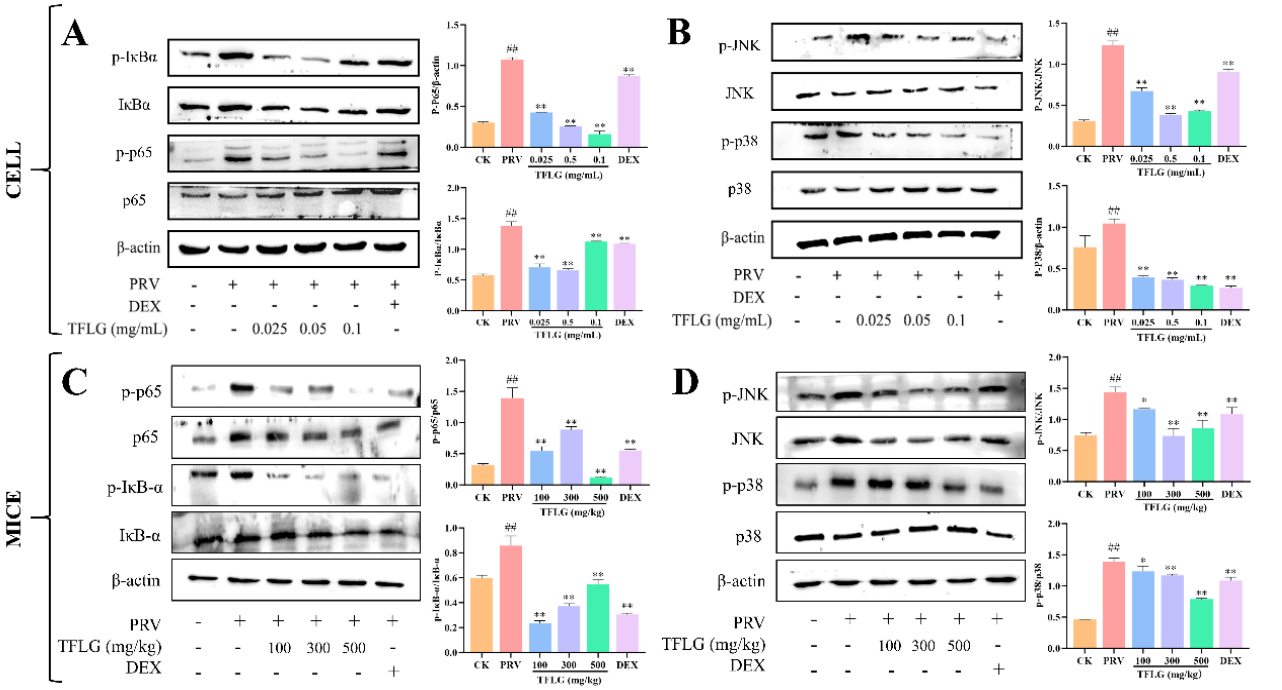

Fig. 4: Effects of TFLG on the phosphorylation levels of proteins associated with the NF-κB and MAPK signaling pathways in (A and B) RAW264.7 cells and (C and D) mouse lungs. The indications of significant differences are shown in Fig. 1.

Analysis of differential metabolites: In RAW264.7 cells, 322 metabolites were increased and 92 were decreased in the CK group compared to PRV group (Fig. 5A). In the PRV group, 7 metabolites were upregulated and 54 were downregulated compared with the TFLG group (Fig. 5B). In mouse serum, 34 metabolites were increased and 130 were decreased in the CK group than those in PRV group (Fig. 5C), whereas 85 upregulated and 57 downregulated metabolites were detected in the PRV group than those in TFLG group (Fig. 5D). Heatmaps were then generated to visualize the top 20 differential metabolites in RAW264.7 cells and mouse serum (Fig. 5E-F). Detailed information about these metabolites is provided in Tables S4 and S5.

Comparison of the cell and serum metabolomics, fumarate, malate and glutamine were identified as shared metabolites, suggesting the TCA cycle as a common metabolic pathway associated with the effects of TFLG against PRV-induced inflammatory *in-vitro* and *in-vivo*. Functional annotation of the differential metabolites was conducted. These differential metabolites were primarily associated with amino acid metabolism, nucleotide metabolism, lipid metabolism, carbohydrate metabolism, and energy metabolism (Fig. 5G-H).

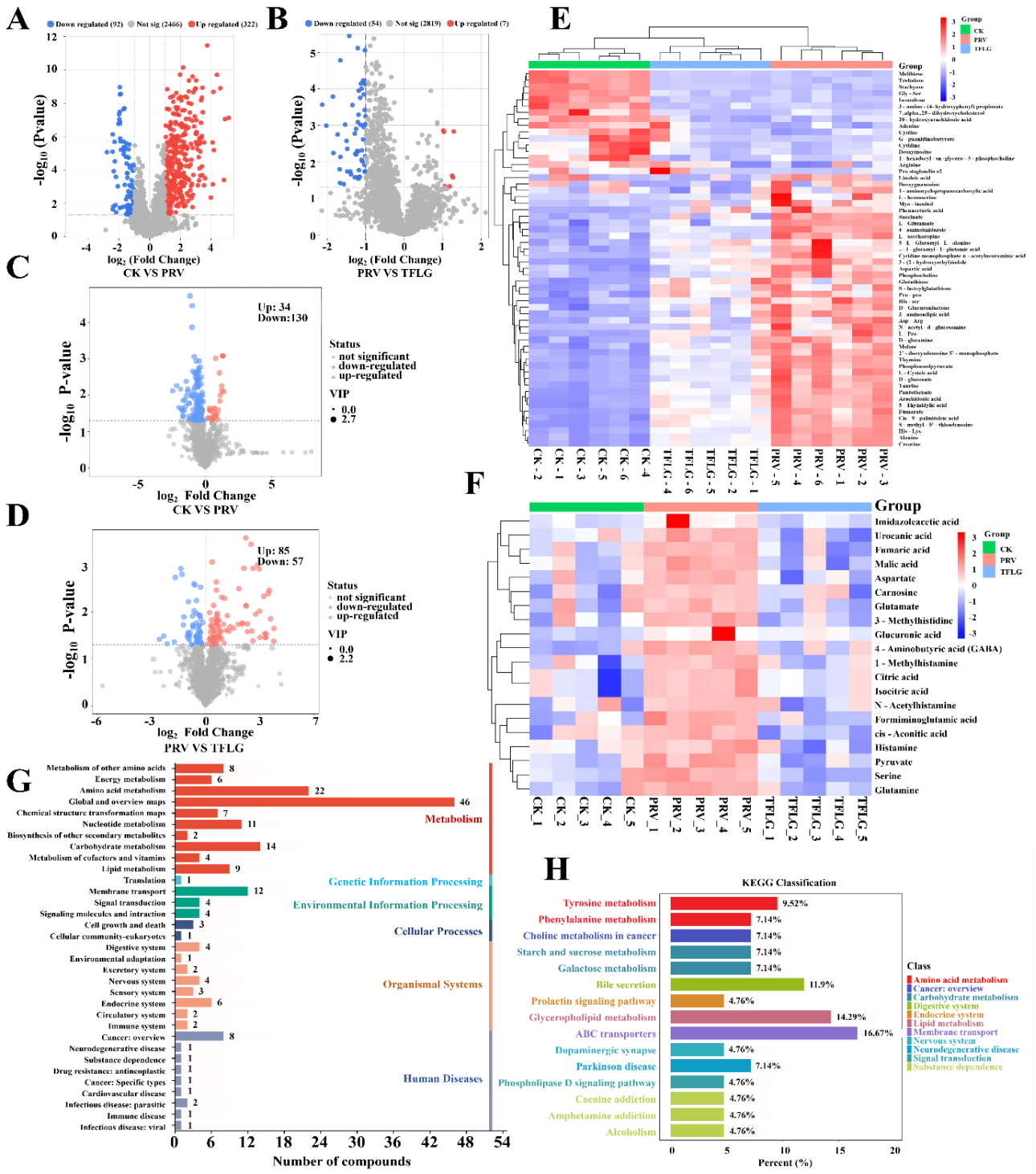

Fig. 5: Effects of TFLG on differential metabolites: (A and B) volcano plots of differential metabolites in RAW264.7 cells; (C and D) volcano plots of differential metabolites in mouse serum; (E) and (F) heatmaps of differential metabolites in RAW264.7 cells and in mice serum, respectively; (G) and (H) functional pathways of differential metabolites in RAW264.7 cells and in mice serum, respectively.

Function pathways analysis: Pathways analysis identified 10 potential metabolic pathways altered by PRV infection in cells, including alanine, taurine and hypotaurine metabolism, the citric acid cycle, arachidonic acid metabolism and glycolysis (Fig. 6A-B). TFLG markedly changed PRV-induced metabolism associated with the cellular inflammatory response, particularly in pathways related to the citric acid cycle, linoleic acid metabolism, taurine and hypotaurine metabolism, glycolysis and arachidonic acid metabolism (Fig. 6C-D). In mouse serum, PRV-induced changes in the inflammatory metabolism were mainly enriched in histidine metabolism, glycerophospholipid metabolism, and alanine (Fig 6E-F). However, TFLG significantly improved these metabolic disturbances through signaling pathways such as the TCA cycle (Fig 6G-H). *In-vitro* and *in-vivo* metabolomic results showed distinct metabolic pathways changes, but both involved the TCA cycle, indicating that TFLG may alleviate PRV-induced inflammation partly by improving TCA cycle-related energy metabolism.

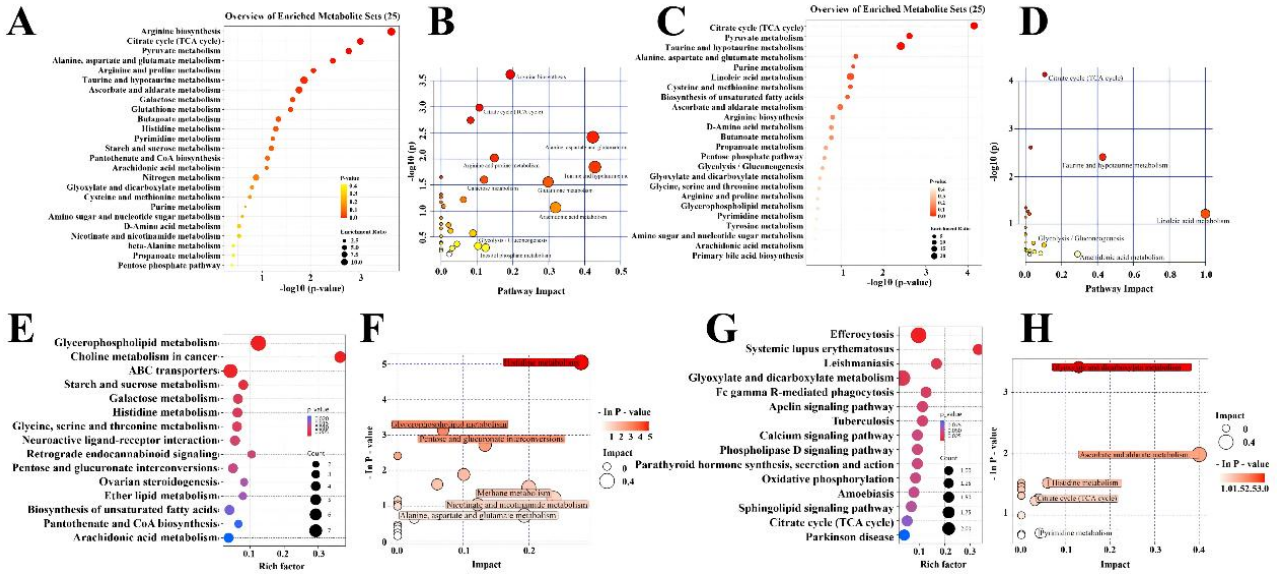

Fig. 6: Analysis of differential metabolic pathways: (A, B) CK-PRV and (C, D) PRV-TFLG comparisons in RAW264.7 cells; (E, F) CK-PRV, (G, H) PRV-TFLG comparisons in mouse serum.

Correlation analysis: Correlation analysis was performed by integrating inflammatory cytokines, cytokine-related gene expression, NF-κB and MAPK pathways proteins, and differential metabolites from *in vitro* and *in vivo* samples. Pearson correlation coefficients were calculated to assess pairwise relationships among all variables, with results visualized using a heat map. *TNF-α* mRNA, *IL-1β* mRNA, *IL-6* mRNA, p-p65, and p-p38 exhibited significant positive correlations with metabolites including arachidonic acid, fumaric acid, malic acid, taurine, creatine, proline, histidine, serine, and glutamic acid. By contrast, *IL-10* mRNA showed a highly significant negative correlation with these metabolites. Additionally, *IL-10*, *TNF-α*, p-JNK and p-p38 collectively demonstrated highly significant correlations with pyruvic acid, serine, and glutamine (P≤0.01) **(**Fig. 7**)**.

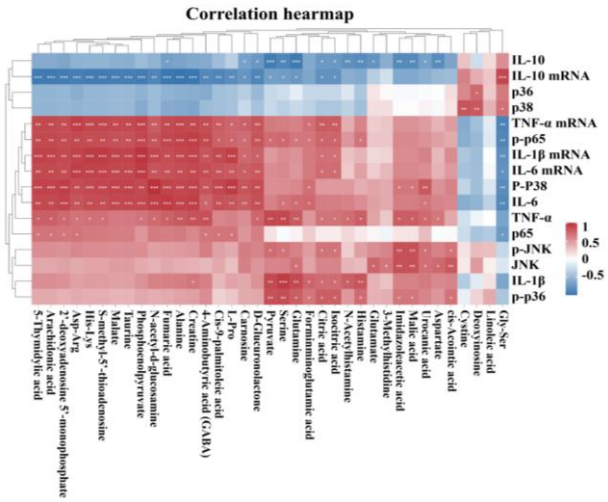

Fig. 7: Correlation analysis.

DISCUSSION

Many plant components can protect against PRV infection. For instance, *Dandelion* aqueous extract can interfere with PRV adsorption and replication, reducing viral gene expression and regulating cytokine production (Cai *et al.,* 2022). Resveratrol protects mice from PRV-induced encephalitis by modulating microglia and neuronal responses (Chen *et al.,* 2023c). Kaempferol conferred protection in PRV-challenged mice by decreasing viral DNA burden and mitigating tissue damage, thereby increasing the survival rate of mice by 22.22%(Lai *et al.,* 2021; Chen *et al.,* 2022). Unlike these compounds, LGH is frequently applied in treating inflammation-related diseases, but its role in treating PRV-infected inflammation has not been investigated. Previous studies have indicated that LGH can elevate the proportion of $CD4^+/CD8^+$ T cells both *in-vitro* and *in-vivo*, reduce *IFN-γ*, *TNF-α*, and *IL-1β* genes expression, and inhibit inflammatory response induced by respiratory syncytial virus (Chen *et al.,* 2019). In this study, we first optimized viral inoculation doses and drug concentrations. Results showed that TFLG showed good safety for cells within the experimental concentration range. PRV infection induced a systemic inflammatory phenotype in mice. Blood-cell analysis showed elevated white blood cells counts, with higher proportions of neutrophils, lymphocytes and monocytes in PRV-infected mice. These changes were accompanied by altered organ indices, as well as the infiltration of inflammatory cells. TFLG treatment reversed these injuries by reducing inflammatory blood cell responses, improving organ indices, and alleviating inflammatory infiltration.

TFLG further altered the secretion of PRV-induced inflammatory in RAW264.7 cells and mice. IL-1β, IL-6 and TNF-α are major cytokines that promote the production of immune cells, inflammatory amplification and tissue injury (Candelli *et al.,* 2025; Liu *et al.,* 2025). TFLG reduced the secretion and mRNA expression of IL-1β, IL-6 and TNF-α, revealing its inhibitory effect on PRV-induced inflammation. At the same time, TFLG increased the expression of IL-10 (P<0.01). IL-10 can suppress the expression of pro-inflammatory genes through limiting NF-κB nuclear translocation and MAPK phosphorylation (Carlini *et al.,* 2023; Mishra *et al.,* 2025). Besides, NO is continuously generated during inflammatory responses and can contribute to tissue damage. Modulating inducible nitric oxide synthase (iNOS) activity has been considered a

therapeutic strategy for chronic inflammation (Kim and Lee, 2025). TFLG significantly reduced NO levels, which could be related to the suppression of iNOS expression and/or enzymatic activity, but further experiments are required to confirm this mechanism. Accordingly, TFLG appears to alleviate PRV-induced inflammation *via* a dual function: inhibition of pro-inflammatory cytokines and enhancement of anti-inflammatory signaling.

These cytokine changes were consistent with the regulation of NF-κB and MAPK signaling pathways. NF-κB classical inflammatory pathways activated by diverse pathogenic and stress signals (Li *et al.,* 2026). In this work, TFLG reduced p65 and IκB-α phosphorylation, suggesting the decrease of NF-κB activation. The MAPK pathways can facilitate the secretion of inflammatory cytokines, particularly through p38 and JNK pathways. p38 and JNK can promote the production of IL-1β and TNF-α, whereas pro-inflammatory cytokines can further activate p38 MAPK (Suriyaprom *et al.,* 2023). In this study, TFLG inhibited JNK and p38 phosphorylation, which may explain the decrease of IL-1β, IL-6 and TNF-α. Notably, MAPK is also involved in the regulation of *IL-10* expression, and NF-κB activation can stimulate IL-10 production (Carlini *et al.,* 2023). The elevation in IL-10 on TFLG treatment may represent a compensatory anti-inflammatory response associated with NF-κB/MAPK pathways. This finding is consistent with the ELISA, which revealed lower pro-inflammatory cytokine levels and higher IL-10 production after TFLG treatment.

Since the inflammatory process leads to the release of a large number of inflammatory factors and significantly increases energy demand, the production of glycolysis and the TCA cycle may be effective targets for balancing chronic inflammatory diseases (Soto-Heredero *et al.,* 2020). For instance, succinate, a key TCA cycle intermediate, can also act as a pro-inflammatory metabolite (Wang *et al.,* 2019). Through metabolomics analysis, we found that the levels of cysteine, serine, alanine and enopyruvate were reduced upon TFLG treatment. TFLG may suppress glycolytic activity and reduce formation of pyruvate-derived citrate, which could impair the TCA cycle and lower the energy supply required for inflammatory activation. Consistently, several TCA cycle intermediates with potential pro-inflammatory roles were also reduced after TFLG treatment.

Histidine has been reported to limit pro-inflammatory cytokine production and serve as a precursor for carnosine synthesis together with β-alanine (Saadati *et al.,* 2024; Barbati *et al.,* 2025). TFLG did not markedly change histidine levels, but it reduced histamine, a downstream metabolite of histidine. Histamine can activate histamine receptors and promote inflammatory responses. It can also increase phosphorylated p38 and JNK protein levels, thereby activating NF-κB and MAPK signaling. Furthermore, glutamine-derived metabolites were also involved in the regulatory effect of TFLG. α-Ketoglutarate, generated from glutamine and glutamate metabolism, is an important metabolic intermediate linked to macrophage activation. Studies reported that α-ketoglutarate can promote the polarization of M1 macrophage and increase TNF-α, IL-1β and IL-6 levels (Cai *et al.,* 2024). In this study, glutamate, isocitrate, and α-ketoglutarate decreased after TFLG treatment, which could reduce the activation of pro-inflammatory factors. Therefore, TFLG may attenuate PRV-induced inflammatory injury through a TCA metabolic pathway. The decrease in histamine may weaken p38/JNK activation and reduce MAPK-mediated inflammatory signaling. Meanwhile, reduced α-ketoglutarate may limit macrophage inflammatory activation and suppress pro-inflammatory cytokine production. These metabolic changes were consistent with the inhibition of NF-κB/MAPK pathways, therefore suppressing NO, IL-1β, IL-6 and TNF-α secretion, while increasing IL-10 production (Fig. 8).

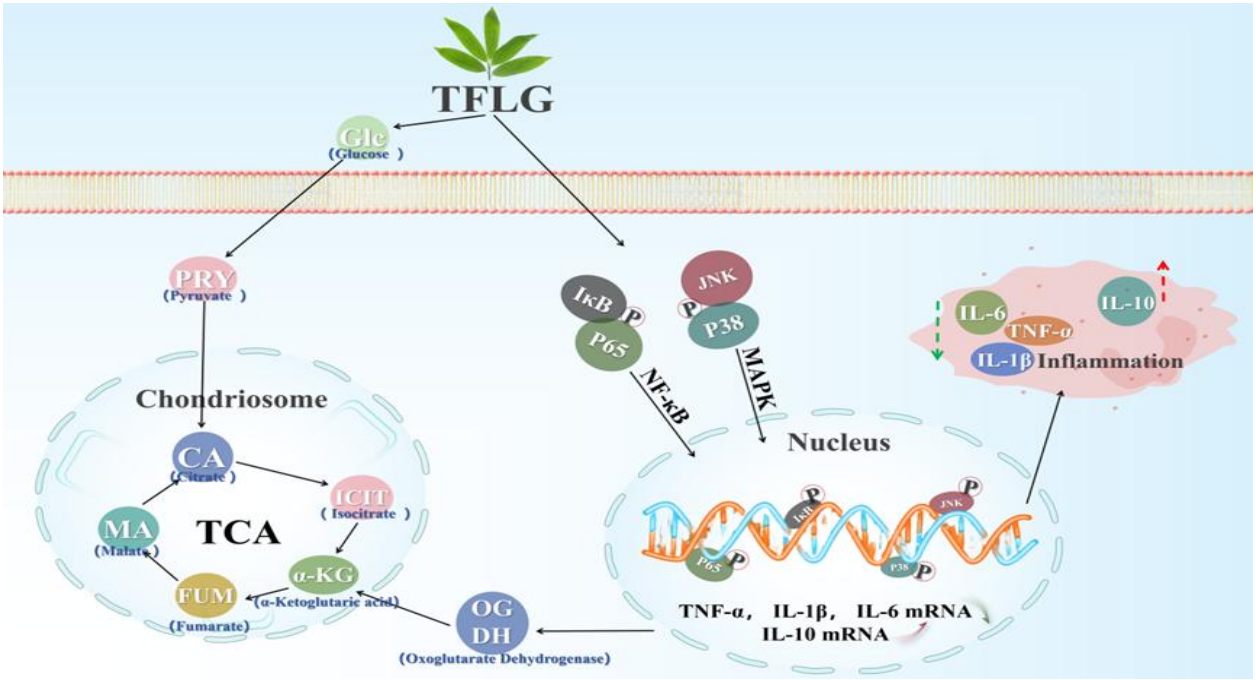

Fig. 8: Proposed mechanism by which TFLG regulates PRV-induced inflammatory metabolism. TFLG may be combined with membrane associated receptor proteins to inhibit MAPK and NF-κB signaling, thereby reducing phosphorylation-dependent inflammatory activation. TFLG also suppresses pyruvate and OGDH activity in TCA cycle, leading to the limit of MAPK and NF-κB activation.

Conclusions: This study reveals that TFLG alleviates inflammatory injury induced by PRV in both cell and mice models. TFLG reduced the production of NO and the secretion of pro-inflammatory cytokines. It also increased IL-10 and improved PRV-induced changes in inflammatory cells and immune organ indices. Furthermore, TFLG suppressed NF-κB and MAPK signaling pathways by blocking the phosphorylation of p65, IκBα, p38 and JNK. More importantly, metabolomic analysis revealed that TFLG not only suppressed inflammatory responses but changed PRV-disrupted metabolic homeostasis. The protective effect of TFLG was closely linked to TCA cycle. TFLG regulated the glutamate-α-ketoglutarate route, which relates to inflammatory response with the TCA cycle. These metabolic changes may contribute to the inhibition of NF-κB/MAPK signaling, thereby decreasing the production of pro-inflammatory cytokines and enhancing anti-inflammatory responses. This study provides evidence that TFLG may serve as a natural anti-inflammatory candidate for controlling virus-associated inflammatory damage.

Ethical statement: All animal procedures were authorized by the Experimental Animal Ethics Committee of Guizhou University (EAE-GZU-2023-E073) and complied with its relevant guidelines and regulations.

Conflicts of interest: The authors declare no conflicts of interest.

Authors Contribution: ZC: Designed and implemented the overall experiments, analyzed the experimental data and drafted the manuscript; LX: Assisted in experimental operation and data analysis; CL: Guided the experimental direction, and formulated and optimized the experimental schemes; CA: Supervised the overall research direction of this study; CZ: Participated in data analysis and assisted with manuscript revision; CY, LQ: Participated in the whole experiment, and was primarily responsible for data analysis and figures plotting; YL: Assisted in the feeding and dissection of laboratory animals; SX, YJ: experimental design, guided data analysis, and financial support

Funding statement: National Natural Science Foundation of China (32661002, 32202854), the Guizhou Provincial Basic Research Program (Natural Science) (No. QKHJC-MS-2025-586), the Guizhou University Natural Sciences Project for Special Post (Leading Group 2024-12), Hundred Thousand Million Leading Talent Teams of Guizhou Province (BQW2025-004), Yunnan Key Laboratory of Veterinary Etiological Biology (202449CE340019).

Data Availability Statement: Data will be made available on request.

REFERENCES

Barbati SA, Carota G, Partsinevelos K, *et al.*, 2025. Preclinical evidence and therapeutic perspectives on carnosine for the treatment of neurodegenerative disorders. Aims Neuroscience 4(12):444-513.

Bo Z, Li X, 2022. A review of Pseudorabies virus variants: genomics, vaccination, transmission, and zoonotic potential. Viruses-Basel 5(14):1003.

Bo Z, Wang S, Li X, *et al.*, 2023. Ginkgolic acid inhibits the replication of pseudorabies virus *in-vitro* and *in-vivo* by suppressing the transcription of viral late genes. Research in Veterinary Science 164:105033.

Cai X, Shao Y, Wang Z, *et al.*, 2022. Antiviral activity of dandelion aqueous extract against pseudorabies virus both *in-vitro* and *in-vivo*. Frontiers in Veterinary Science 9:1090398.

Cai Z, Li W, Hager S, *et al.*, 2024. Targeting PHGDH reverses the immunosuppressive phenotype of tumor-associated macrophages through α-ketoglutarate and mTORC1 signaling. Cellular and Molecular Immunology 5(21):448-465.

Candelli M, Sacco Fernandez M, Rozzi G, *et al.*, 2025. The Interleukin network in sepsis: from Cytokine storm to clinical applications. Diagnostics (Basel, Switzerland) 22(15):2927.

Carlini V, Noonan DM, Abdalalem E, *et al.*, 2023. The multifaceted nature of IL-10: regulation, role in immunological homeostasis and its relevance to cancer, COVID-19 and post-COVID conditions. Frontiers in Immunology 14:1161067.

Chen LF, Zhong YL, Luo D, *et al.*, 2019. Antiviral activity of ethanol extract of *Lophatherum gracile* against respiratory syncytial virus infection. Journal of Ethnopharmacology 242:111575.

Chen X, Wang R, Hu H, *et al.*, 2022. Antiviral effect of an extract from *Kaempferia galanga* L. rhizome in mice infected with pseudorabies virus. Journal of Virological Methods 307:114573.

Chen X, Xue J, Zou J, *et al.*, 2023a. Resveratrol alleviated neuroinflammation induced by pseudorabies virus infection through regulating microglial M1/M2 polarization. Biomedicine and Pharmacotherapy 160:114271.

Chen Y, Chen C, Lai K, *et al.*, 2023b. Anti-inflammatory and antiviral activities of flavone *C*-glycosides of *Lophatherum gracile* for COVID-19. Journal of Functional Foods 101:105407.

Chen YL, Chen CY, Lai KH, *et al.*, 2023c. Anti-inflammatory and antiviral activities of flavone *C*-glycosides of *Lophatherum gracile* for COVID-19. Journal of Functional Foods 101:105407.

Chen J, Zhao G, Yang Y, *et al.*, 2025. Pseudorabies virus induces natural killer cell depletion by GSDMD-mediated inflammation and pyroptosis to promote infection and lung injury. Journal of Virology 8(99):e41525.

Gao W, Zhang M, Zhu Z, 2025. The prevalence of pseudorabies virus in China from 2010 to 2024: a systematic review and meta-analysis. BMC Veterinary Research 1(21):513.

Kim ME, Lee JS, 2025. Advances in the regulation of inflammatory mediators in Nitric Oxide synthase: Implications for Disease Modulation and Therapeutic Approaches. International Journal of Molecular Sciences 3(26):1204.

Lai KH, Chen PJ, Chen CC, *et al.*, 2021. *Lophatherum gracile* Brongn. attenuates neutrophilic inflammation through inhibition of JNK and calcium. Journal of Ethnopharmacology 264:113224.

Liu P, Hu D, Yuan L, *et al.*, 2022a. Metabolomics analysis of PK-15 cells with Pseudorabies virus infection based on UHPLC-QE-MS. Viruses-Basel 6(14):1158.

Liu Q, Kuang Y, Li Y, *et al.*, 2022b. The epidemiology and variation in Pseudorabies virus: A continuing challenge to pigs and humans. Viruses-Basel 7(14):1463.

Li Q, Liu Y, Bao H, *et al.*, 2024. The Application of *Lophatherum gracile* brongn flavonoids in wheat flour products: Effects on the structural and functional characteristics of wheat dough. Foods 16(13): 2556.

Li X, Luo Z, Hu T, *et al.*, 2025. Exploring the anti-inflammatory effects of total flavonoids from *L. gracile* on LPS-induced inflammation: An integrated approach combining network pharmacology, molecular docking, and experimental validation. International Immunopharmacology 161:115027.

Li Y, Jiang H, Chen R, *et al.*, 2026. NF-κB Signaling as a central driver of cancer Cachexia, Cancers 4(18):557.

Liu M, Chen R, Zheng Z, *et al.*, 2025. Mechanisms of inflammatory microenvironment formation in cardiometabolic diseases: molecular and cellular perspectives. Frontiers in Cardiovascular Medicine 11:1529903.

Mishra B, Bachu M, Yuan R, *et al.*, 2025. IL-10 targets IRF transcription factors to suppress IFN and inflammatory response genes by epigenetic mechanisms. Nature Immunology 5(26):748-759.

Saadati S, Kabthymer RH, Aldini G, *et al.*, 2024. Effects of carnosine and histidine-containing dipeptides on biomarkers of inflammation and oxidative stress: a systematic review and meta-analysis. Nutrition Reviews 12(82):1696-1709.

Song C, Wei Q, Shen H, *et al*, 2025. Therapeutic potential of *Glycyrrhiza* polysaccharides in pseudorabies virus infection: immune modulation, antioxidant activity, and gut microbiota restoration. Frontiers in Veterinary Science 12:1679013.

Soto-Heredero G, Gomez DLHM, Gabande-Rodriguez E, *et al.*, 2020. Glycolysis - a key player in the inflammatory response. Febs Journal 16(287):3350-3369.

Suriyaprom S, Srisai P, Intachaisri V, *et al.*, 2023. Antioxidant and anti-inflammatory activity on LPS-Stimulated RAW 264.7 Macrophage Cells of White Mulberry (*Morus alba* L.) Leaf Extracts. Molecules (Basel, Switzerland) 11(28):4395.

Tang Q, Shao M, Wang Y, *et al.*, 2015. Simultaneous determination of 10 bioactive components of *Lophatherum gracile* brongn by HPLC-DAD. Journal of Chromatographic Science 6(53):963-967.

Vervaeke A, Lamkanfi M, 2025. MAP Kinase Signaling at the crossroads of inflammasome activation. Immunological Reviews 1(329):e13436.

Wang X, Liu R, Qu X, *et al.*, 2019. alpha-Ketoglutarate-activated NF-kappaB signaling promotes compensatory Glucose uptake and brain tumor development. Molecular Cell 1(76):148-162.

Xu L, Zhang Y, Tao Q, *et al.*, 2024. Transcriptome and metabolome analysis reveals PRV XJ delgE/gI/TK protects intracranially infected mice from death by regulating the inflammation. Frontiers in Microbiology15:1374646.

Yang M, Feng K, Li Y, *et al.*, 2026. Research progress on anti-inflammatory and antioxidant mechanism of artemether based on MAPK/NF-κB signaling pathways. International Journal of Molecular Sciences 10(27):4607.

Yao J, Li J, Gao L, *et al.*, 2022. Epidemiological investigation and genetic analysis of pseudorabies virus in Yunnan Province of China from 2017 to 2021. Viruses-Basel 5(14): 895.

Zhuang L, Gong J, Shen J, *et al.*, 2025. Advances in molecular epidemiology and detection methods of pseudorabies virus. Discover Nano 1(20):45.

Zhou Q, Zhang L, Lin Q, *et al.*, 2023. Pseudorabies virus infection activates the TLR-NF-κB Axis and AIM2 inflammasome to enhance inflammatory responses in mice. Journal of Virology 3(97):e323.